

The dependence between forces and dissipation rates mediating dynamic self-assembly†

Konstantin V. Tretiakov,^{ac} Kyle J. M. Bishop^a and Bartosz A. Grzybowski^{*ab}

Received 2nd July 2008, Accepted 7th November 2008

First published as an Advance Article on the web 12th January 2009

DOI: 10.1039/b811254a

Dynamic self-assembly (DySA) outside of thermodynamic equilibrium underlies many forms of adaptive and intelligent behaviors in both natural and artificial systems. At the same time, the fundamental principles governing DySA systems remain largely undeveloped. In this context, it is desirable to relate the forces mediating self-assembly to the nonequilibrium thermodynamics of the system—specifically, to the rate of energy dissipation. In this paper, numerical simulations are used to calculate dissipation rates in a prototypical, magneto-hydrodynamic DySA system, and to relate these rates to dissipative forces acting between the system's components. It is found that (i) dissipative forces are directly proportional to the gradient of the dissipation rate with respect to a coordinate characterizing the steady-state assemblies, and (ii) the constant of proportionality linking these quantities is a characteristic time describing the response of the system to small, externally applied perturbations. This relationship complements and extends the applicability of Prigogine's minimal-entropy-production formalism.

1. Introduction

Self-assembly (SA)^{1,2} is a process, in which discrete components organize spontaneously—that is, without any human intervention—into ordered and/or functional super-structures.¹ Long perfected through evolution, SA in biological systems provides the means by which various proteins organize into multiprotein complexes,³ lipids into cellular membranes, cells into tissues, bacteria into colonies,^{4,5} and higher organisms into swarms,⁶ schools,⁷ or flocks.⁸ Science and technology have long recognized the promise of self-assembly (SA) as a versatile way of building large structures from small objects and as an elegant alternative to “top-down” fabrication methods. Self-assembled monolayers,^{9,10} metal-organic frameworks,¹¹ nanostructured materials,¹² photonic crystals,¹³ self-building electric circuits,¹⁴ “magnetic hole” effect,¹⁵ and polymer sacs/membranes¹⁶ attest to the experimental skill and creativity with which scientists and engineers can currently harness the power of SA to build stable, equilibrium structures and materials. In this effort, they are aided by equilibrium thermodynamics, which tells us that equilibrium assemblies correspond to the minima of appropriate thermodynamic potentials (Fig. 1a). Although finding predictive relationships between the interactions acting in a self-assembling system and its final structure might be difficult, it is, at least in principle, possible.

This convenient situation changes dramatically when the SA processes occur—like in most animate systems—away from thermodynamic equilibrium such that assemblies that form

require constant supply of energy which they continuously dissipate in order to maintain the organized state (Fig. 1b). As argued in detail elsewhere,² these dissipative or “dynamic” SA (DySA) systems have the capacity to exhibit adaptability, self-healing, and even self-replication, and can therefore be considered as candidates for the “smart” materials of the future. For the time being, however, there are only a handful of man-made, model DySA systems (Fig. 2) and virtually no theoretical principles describing their behaviors and/or the relationship(s) between energy dissipation and the mode(s) of system's organization. This article suggests one such principle that relates variations in the rate of energy dissipation to the magnitudes of interparticle forces.

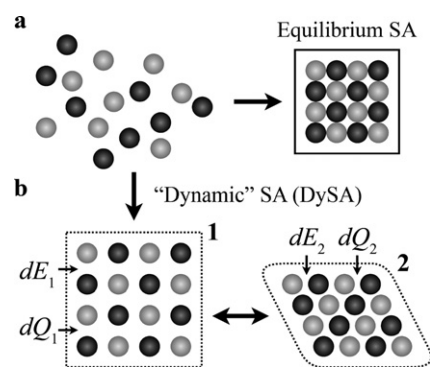


Fig. 1 Equilibrium vs. dynamic self-assembly. (a) In equilibrium self-assembly, components organize to minimize an appropriate thermodynamic potential. The resulting assembly is closed from its surroundings in the sense that there are no systematic flows of mass, momentum, or energy into or out of the system. (b) In nonequilibrium or “dynamic” self-assembly (DySA), the structures that form are maintained only through a constant supply of energy, dE , which is subsequently dissipated as heat, dQ , through the components' interactions with each other and with their environment. Depending on the rate of energy input, a DySA system may adopt different configurations with qualitatively different “modes” of dissipation.

^aDepartment of Chemical and Biological Engineering, 2145 Sheridan Road, Evanston, Illinois 60208, USA. E-mail: grzybor@northwestern.edu

^bDepartment of Chemistry Northwestern University, 2145 Sheridan Road, Evanston, Illinois 60208, USA

^cInstitute of Molecular Physics, Polish Academy of Sciences, Smoluchowskiego 17/19, 60-179 Poznań, Poland

† This paper is part of a *Soft Matter* theme issue on Self-Assembly. Guest editor: Bartosz Grzybowski.

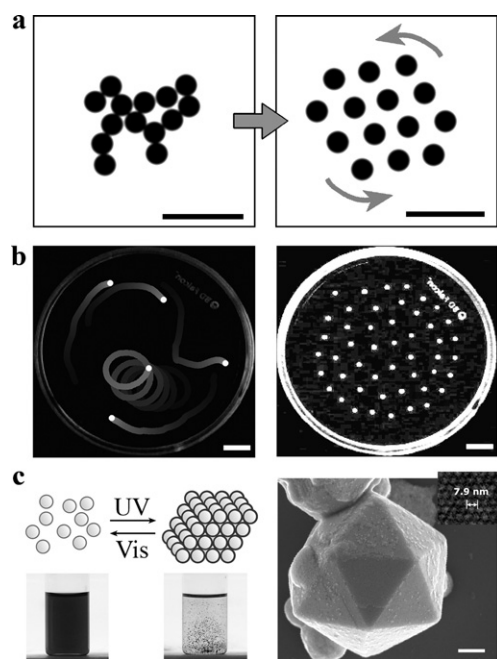


Fig. 2 Examples of dynamic self-assembly (DySA). (a) In magneto-hydrodynamic DySA,^{23–25} millimetre-sized magnetic particles rotate at a fluid–air interface and organize to form dynamic, open-lattice assemblies, in which repulsive hydrodynamic interactions are balanced by a confining magnetic potential. At equilibrium (*i.e.*, no energy input), the pieces float at a fluid–air interface and clump together *via* capillary forces (*left*). Introducing a nonequilibrium driving force (*right*)—here, using a rotating magnetic field—the system “comes to life” creating a dynamic assembly maintained by vortex–vortex interactions (see Fig. 3 for more details). Scale bars = 5 mm. (b) In DySA *via* dynamic surface tension,³⁷ hydrogel particles doped with camphor and floating at a water–air interface move about spontaneously (*left*) due to fluid flows generated by surface tension gradients. At sufficiently high densities (*right*), the particles organize into an open lattice due to repulsive interactions caused by the Marangoni-type flows. Scale bars = 5 mm. (c) At the nanoscale, DySA has been used to build dynamic nanoparticle (NP) assemblies, in which the interactions between proximal NPs are mediated by photoisomerizable azobenzene molecules tethered to the NPs’ surface.^{38,39} NPs organize reversibly to form crystalline assemblies (*right*) only under UV irradiation, which maintains a nonequilibrium distribution of the polar *cis* isomers responsible for the attractive interactions between NPs. In the absence of UV “food”, the crystals fall part. Scale bar = 200 nm.

From a theoretical perspective, DySA structures belong to a broad class of nonequilibrium (NE) steady-state systems (or “dissipative structures”¹⁷), in which the production of entropy (*i.e.*, dissipation of useful energy) directs the emergence of order (*cf.* Fig. 1b). Such dissipative structures can be understood qualitatively as nature’s “optimal” solutions for the efficient degradation of thermodynamic gradients *via* dissipative processes. A generalized quantitative description, however, remains lacking. For small displacements from equilibrium,¹⁸ it is well established that nonequilibrium systems evolve to steady-state configurations that minimize entropy production (MEP) subject to the externally imposed NE constraints (*e.g.*, an imposed temperature gradient).¹⁹ Beyond this so-called linear regime of NE thermodynamics, no general variational principle exists, and one must rely on specific kinetic models to describe a system’s dynamics.

The situation is further complicated in the context of DySA, in which the forces between *discrete* components are mediated by some external medium (usually, a fluid), into which the supplied energy is ultimately dissipated. To illustrate these difficulties, consider the specific class of nonequilibrium phenomena described by Newtonian hydrodynamics. For steady viscous flows with specified boundary conditions, the minimum energy dissipation theorem²⁰ states that the velocity field satisfying the Stokes equations (*i.e.*, at Reynolds number, $Re = 0$) dissipates less energy than any other velocity field consistent with the boundary conditions and the continuity equation. For particulate flows, however, in which one or more solid objects move freely or under some applied constraints within the fluid domain, it is not clear if the same theorem applies.²¹ Nevertheless, there exists some evidence in the context of low (but finite) Reynolds number hydrodynamics that the forces imparted on the particle(s) by the fluid act to minimize the total rate of viscous dissipation, subject to constraints imposed on the particle(s). For example, a sphere falling through a vertical cylinder filled with a viscous fluid adopts a radial position consistent with this minimum energy dissipation criterion.²¹ Similarly, a cylinder rotating within another cylinder and separated by a viscous fluid will be forced to a coaxial configuration, again minimizing the dissipation rate.²² These examples suggest that certain fluidic forces are related to the viscous dissipation rate and vanish when that rate is minimal. Can this reasoning be extended to DySA, and can the dissipative forces mediating self-assembly be related to the total rate of energy dissipation (or entropy production) of the system? Also, many (if not, most) DySA systems involve both dissipative and conservative interactions, the latter being independent of energy dissipation (for examples, see ref. 2). Can dissipative forces still be related to energy dissipation in such cases?

These questions are both fascinating and difficult to answer, since there are very few systems available that are complex enough to exhibit DySA and yet simple enough to allow exact calculation of dissipation rates. A class of magneto-hydrodynamic DySA systems combining dissipative vortex–vortex forces with conservative magnetic interactions (Fig. 2a and Fig. 3) is a rare example where both theoretical analysis and experimental validation are possible. Therefore, we focus our present study on this specific realization of DySA and investigate the relationship between the hydrodynamic forces mediating SA and the viscous dissipation rate. Through numerical simulations, we find that the dissipative forces, F_D , are related to variations in the dissipation rate, ϵ , by a characteristic time, τ_{ss} , describing the response of the steady-state configuration to external perturbations. Moreover, the steady-states into which the system ultimately settles are described by the balance of dissipative and non-dissipative forces, and do not necessarily minimize dissipation rates, as would be predicted by the Prigogine’s MEP rule. Thus, the proposed relation between forces and dissipation may prove useful in describing the steady-state behaviors of DySA systems beyond the limits of validity for the MEP principle.

2. Magneto-hydrodynamic DySA.^{23–29}

The model DySA system we consider consists of a collection of small, millimetre-sized magnetic particles (typically, polymer pieces loaded with magnetite) floating at a liquid–air interface

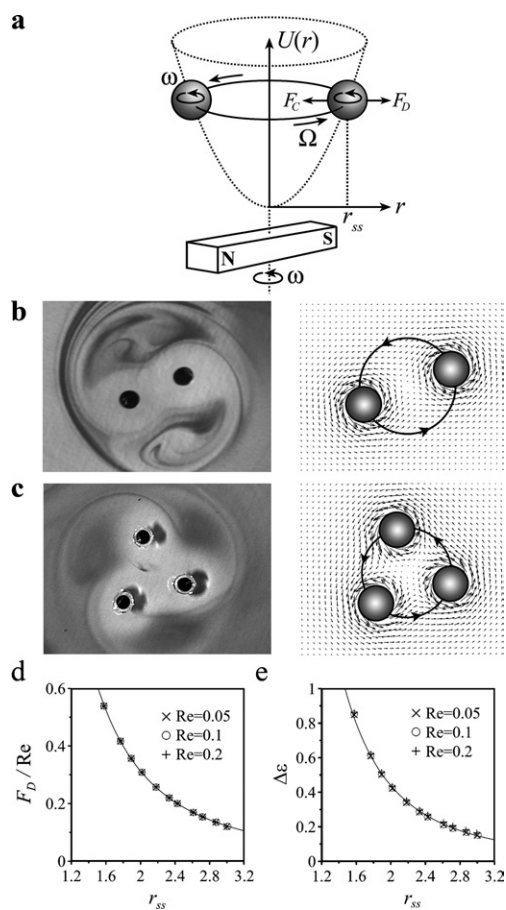


Fig. 3 Modeling of magneto-hydrodynamic DySA. (a) A schematic illustration of the experimental setup. Spherical particles (gray) confined to a liquid–air interface rotate with fixed angular velocity ω equal to that of the rotating bar magnet. This rotation causes the particles to move on a circular trajectory at an angular velocity Ω , which depends on ω [in the Stokes limit, $\Omega = \frac{1}{4}\omega(alr_{ss})^3$]. For finite fluid inertia ($Re \neq 0$), the vortices generated by the spheres induce a repulsive force, F_D , which is balanced at steady-state by conservative magnetic force, $F_C = -\nabla U$, due to the rotating magnet. (b–c) (*left*) Experimental images of the steady-state assemblies of two and three “spinners”; the flows are visualized by injection of a Crystal Violet dye. (*right*) Analogous assemblies calculated numerically; vector flow fields are illustrated by the small arrows, and the circles trace the steady trajectories of the particles. (d) Hydrodynamic force, F_D , divided by the Reynolds number, Re , as a function of the steady-state radial position, r_{ss} , of the spheres. The fact that these three dependencies collapse onto one curve illustrates the linear scaling of F_D with Re . (e) Excess energy dissipation rate, $\Delta\epsilon$, versus the steady-state radial position, r_{ss} . Here, the excess energy dissipation rate is defined as $\Delta\epsilon = \epsilon - \epsilon_\infty$, where $\epsilon_\infty = 16\pi$ is the dissipation rate of the two rotating spheres at infinite separation.

and subject to a magnetic field produced by a rotating permanent magnet (*cf.* Fig. 2a and Fig. 3). Under the influence of this magnet, all particles experience a centrosymmetric, conservative force F_C directed toward the magnet’s axis of rotation and increasing in magnitude with the distance from this axis, r .²³ At the same time, the rotating field causes the particles to spin around their axes at an angular velocity, ω (typically, ~ 10 Hz) equal to that of the magnet. These rotations create vortices in the surrounding fluid and give rise to repulsive vortex–vortex forces,

F_D between the particles. Importantly, these interactions are dissipative such that they persist only as long as the particles are kept spinning. The competition between conservative and dissipative forces evolves the system into open-lattice, steady-state assemblies that slowly orbit the axis of the magnet with an angular velocity, $\Omega \approx 0.01$ Hz. In terms of system energetics, the energy supplied by the rotating magnet is ultimately dissipated through the viscous, hydrodynamic interactions of the particles with the surrounding fluid, and the exact nature of this dissipation determines the organization of the dynamic assemblies.

This system is particularly well suited for our current study for two reasons: (1) its behavior has been carefully characterized through a series of experimental investigations;^{23–29} and the physics underlying the observed phenomena is well established. (2) The system’s dynamics can be modeled theoretically using classical hydrodynamics (*e.g.*, Navier–Stokes equations), in which both the forces and the dissipation rate are unambiguously defined and easily calculated from the fluid’s velocity field. Such a theoretical description has recently been implemented numerically³⁰ and was found to be in excellent agreement with the experimental observations.^{23–25} Overall, magneto-hydrodynamic DySA provides an ideal testing ground for exploring the relationship between energy dissipation and the forces mediating self-assembly.

3. Theoretical description

(i) Dissipative, vortex–vortex forces

We consider the simplest (but see Numerical Simulations) case of two, neutrally buoyant, spherical “spinners” of radius a rotating with a constant angular velocity, ω , in a viscous fluid (Fig. 3).³⁰ The motion of the fluid outside the spheres is governed by the Navier–Stokes equations for an incompressible, Newtonian fluid. Scaling times by ω^{-1} , lengths by a , velocities by $a\omega$, and pressure by $\mu\omega$, where μ is the dynamic viscosity, the dimensionless equations are given by $Re[\partial\mathbf{u}/\partial t + \mathbf{u} \cdot \nabla\mathbf{u}] = -\nabla p + \nabla^2\mathbf{u}$ and $\nabla \cdot \mathbf{u} = 0$, where \mathbf{u} is the velocity field. Here, $Re = \rho a^2 \omega / \mu$ is the Reynolds number describing the relative magnitudes of inertial and viscous effects (in experiments, Re is ~ 0.01 – 1), and ρ is the fluid density. At the surface of the spheres the velocity of the fluid is equal to that of the solid surface (*i.e.*, “no slip” condition), far from the spheres fluid velocity approaches zero.

The fluid motions induced by the rotating spheres give rise to the vortex–vortex forces. Introducing the stress tensor, $\boldsymbol{\sigma} = -p\boldsymbol{\delta} + \boldsymbol{\tau}$, where $\boldsymbol{\delta}$ is the unit tensor, and $\boldsymbol{\tau} = \nabla\mathbf{u} + (\nabla\mathbf{u})'$ is the viscous stress tensor, the force acting on sphere i is given by

$$\mathbf{F}_D^{(i)} = \int_{S^{(i)}} \mathbf{n} \cdot \boldsymbol{\sigma} dS^{(i)},$$

where \mathbf{n} is the unit normal directed out of the sphere’s surface, and integration is carried out over the sphere’s surface. Note that all quantities are dimensionless: stress tensors are scaled by $\mu\omega$ and forces by $\mu\omega a^2$.

(ii) Conservative, magnetic forces

In addition to F_D , the particles also experience “conservative” forces due to magnetic confinement. It has been shown previously that the confining potential is quadratic in the distance from the magnet’s axis of rotation, $U(r) = \beta r^2$, such that the force $F_C = -\nabla U$ scales linearly with r .^{23,25} With these two forces, the

dynamics of the particles are described by, $m^{(i)}d\mathbf{V}^{(i)}/dt = \mathbf{F}_D^{(i)} + \mathbf{F}_C^{(i)}$, where $m^{(i)} = \frac{4}{3}\pi a^3 \rho$ is the mass of particle i , and $\mathbf{V}^{(i)}$ is its velocity.

(iii) Numerical simulations

The Navier–Stokes (NS) equations for the system were solved numerically on 64^3 , 96^3 , 128^3 , and 160^3 grids (to eliminate finite-size effects) using the so-called force coupling method (FCM), in which the solid spheres are approximated by locally distributed body forces acting on the fluid (*cf.* ref. 30 for numerical details and Fig. 3b and c for representative flow fields). This method had been validated extensively through comparison with experiments for various types of fluidic systems,^{31,32} including the DySA spinners.³⁰ Here, we applied this method to investigate various configurations of particles for Reynolds numbers, $Re = 0.05$ to 0.2 . Although computationally demanding even for the case of two particles (about two days on Intel Xeon 5160 processor with the smallest 64^3 space grid and 10^6 iterations to achieve steady-state; for more particles or larger separations, more grid points are needed—*e.g.*, 128^3 grid requires ~ 40 days of computation), the FCM approach enables direct calculation of both the hydrodynamic forces, \mathbf{F}_D , between the particles as well as the viscous dissipation rates, ϵ , for each steady-state configuration. To find the forces, we applied a series of confining potentials of the form $U(r) = \beta r^2$ and integrated the governing NS equations until reaching the steady-state configuration. At steady-state, the two particles follow a circular trajectory of radius, r_{ss} , about the axis of the applied potential, where the value of r_{ss} depends on both the magnitude of the potential, β , and on the Reynolds number, Re . To maintain this steady trajectory, the repulsive hydrodynamic force, \mathbf{F}_D , is exactly balanced by that due to the external potential—*i.e.*, $\mathbf{F}_D = 2\beta r_{ss}$. In this way, we calculated \mathbf{F}_D as a function of the radial position, r , for several steady-state configurations, r_{ss} (*cf.* Fig. 3d). Similarly, the total viscous dissipation rate (scaled by $\mu a^3 \omega^2$), ϵ , was calculated in the usual manner from the steady-state flow field as $\epsilon = \frac{1}{2} \int (\boldsymbol{\tau} \cdot \boldsymbol{\tau}) dV$, where the dot denotes the tensor product, and the integral is carried out numerically over the entire simulation domain (*cf.* Fig. 3e). At steady-state, the kinetic energy of the fluid is constant, and the dissipation rate may also be expressed in terms of the power delivered by the rotating particles as $\epsilon = -\sum_i \mathbf{F}_D^{(i)} \cdot \mathbf{V}^{(i)} + \mathbf{T}_D^{(i)} \cdot \boldsymbol{\omega}^{(i)}$, where $\mathbf{T}_D^{(i)}$ is the torque generated by the fluid on sphere i . To confirm the consistency of the numerical method, we verified that these two approaches for the calculation of ϵ give the same results. Furthermore, in the case of an isolated sphere, the numerically calculated ϵ agreed with the Stokes value to within 0.02%.

Results and discussion

(i) Dissipative force, F_D

The repulsive, hydrodynamic force between the particles is a consequence of finite fluid inertia and depends linearly on the Reynolds number, Re , for the range of Re studied here (Fig. 3d). Qualitatively, this force originates from the secondary flows induced about each sphere, whereby the fluid flows in towards the poles of the particles (*i.e.*, along the axis of rotation) and outwards near their equators.³⁰ The radial outflow from each particle thus acts to “push” the particles apart. This

hydrodynamic force, F_D , is repulsive for all separations (*i.e.*, acts in the positive r direction) and decays monotonically to zero as the steady-state separation, r_{ss} , increases to infinity.

(ii) Rate of dissipation, ϵ

The dissipation rate, ϵ , also decreases with increasing particle separation (Fig. 3e) and approaches the value of $\epsilon(r_{ss} \rightarrow \infty) = 16\pi$, in agreement with the analytical solution for two isolated spheres.³⁰ Thus, in the absence of the applied potential, the repulsive hydrodynamic force, F_D , directs the particles to the state of minimal energy dissipation, in accordance with MEP. If, however, the particles are forced together by an applied magnetic potential, the dissipation rate increases due to an increase in the torque, T_D , required to rotate the particles at a constant angular velocity, ω .³³ The steady-state to which the particles evolve is then different from the state of minimal dissipation.

(iii) Heuristics of the F_D vs. ϵ dependence

We are now in position to seek the relationship between the steady-state values of F_D and ϵ . Although the force is always perpendicular to the particles’ velocities, $\mathbf{V}^{(i)}$, and therefore does not contribute explicitly to the steady-state dissipation rate (since $\epsilon = \sum_i \mathbf{F}_D^{(i)} \cdot \mathbf{V}^{(i)} + \mathbf{T}_D^{(i)} \cdot \boldsymbol{\omega}^{(i)}$), the two quantities are related through the flow field of the fluid. Before discussing the simulations, let us first outline the intuitive reasoning behind the results. First, it is reasonable to expect that the relationship we seek should incorporate not the absolute value of ϵ but the variation in the dissipation rate with respect to changes in the steady-state particle configurations (*e.g.*, changes in r_{ss} for two particle systems). The rationale behind this hypothesis is that if the dissipation rate were constant for all possible particle velocities and spatial configurations, there would be no “driving force” to choose any one of them. In addition, in the absence of the conservative forces, one should expect the system to evolve such as to minimize the dissipation rate (as prescribed by MEP). These considerations suggest a relationship between F_D and the negative of the gradient, $-\nabla\epsilon$, which for circular orbits of the particles simplifies to $-d\epsilon/dr_{ss}$. Next, through dimensional analysis, any relationship between F_D and $d\epsilon/dr_{ss}$ will require a quantity with the units of time, which in general may vary from one steady-state to another (*i.e.*, it might depend on r_{ss}). Therefore, the simplest relationship one can postulate is $F_D(r_{ss}) = -\tau_{ss}(r_{ss}) \frac{d\epsilon}{dr_{ss}}$ (Fig. 5); this functional form agrees with the observed behavior that the magnitude of the force vanishes as the dissipation rate approaches its minimum value (for constant ω constraints). In this equation, the key parameter is τ_{ss} , which is some characteristic time describing the various steady-state configurations. Of course, this time should have the same physical meaning for all steady-states and for different Reynolds numbers. Also, by loose analogy to the so-called Lyapunov exponents (or Lyapunov times) used in dynamical systems theory to describe the rate of convergence/divergence of neighboring trajectories, we hypothesize that the characteristic time, τ_{ss} , is related to the evolution of particle trajectories in the vicinity of steady-states.

(iv) Verification and interpretation (Fig. 4 and Fig. 5)

To verify this hypothesis, we analyzed the effects of small external perturbations on the system's steady-states. These perturbations are effected by instantaneously changing³⁵ the parameter β describing the magnetic confinement, $U(r) = \beta r^2$, and allowing the particles to evolve/"relax" toward their new steady-state orbit, r'_{ss} . During this evolution, the speed of the particle changes compared to the unperturbed system, $\Delta V = V' - V$. When the confinement becomes "stronger" (β increases), ΔV initially decreases (Fig. 4c) before ultimately increasing to the higher rate of the new steady-state ($r'_{ss} < r_{ss}$); if the potential becomes weaker (β decreases), the particles initially speed up before settling to a lower velocity expected for the $r'_{ss} > r_{ss}$ orbit. Since the phenomena involved in both situations are analogous, let us focus on the $r'_{ss} < r_{ss}$ case. Here, the initial decrease in

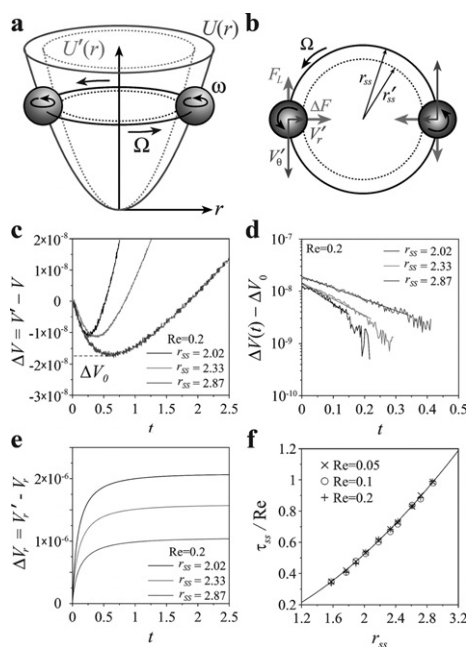


Fig. 4 Results of the numerical simulations. (a) A schematic illustration of the perturbation used in the calculation of the characteristic times, τ_{ss} . The system—initially, at steady-state (solid curve) determined by the potential $U(r)$ —is perturbed by the instantaneous application of a new potential $U'(r)$ and subsequently evolves towards a new steady-state trajectory (dashed curve). (b) The origin of the inertial lift force, F_L , caused by the perturbation. Upon changing the potential from U to U' , the radial forces on the particle are no longer balanced, such there is a net force, $\Delta F = F_C - F_D$, pushing the particles towards the origin. The resulting radial velocity component, V_r' , creates a lift force, $F_L = \omega \times V_r$, which initially decreases the tangential velocity, V_θ , relative to the unperturbed trajectory. (c) Difference in the particle speeds between the perturbed and unperturbed particle trajectories as a function of time. (d) Evaluation of the characteristic time, τ_{ss} , from the semi-logarithmic plot of $\Delta V(t) - \Delta V_0$ vs. time. Within this short time interval, the calculated curve is well approximated by an exponential dependence $\Delta V(t) - \Delta V_0 \approx \exp(-t/\tau_{ss})$. Here, we present three typical curves for the characteristic time; the other >20 analyzed curves have the same characteristics. (e) Difference of radial velocity components, $V_r' - V_r$, for the perturbed and unperturbed particle trajectories plotted as a function of time. (f) Characteristic time scaled by Re as a function of the steady-state radial position, r_{ss} , of the spheres.

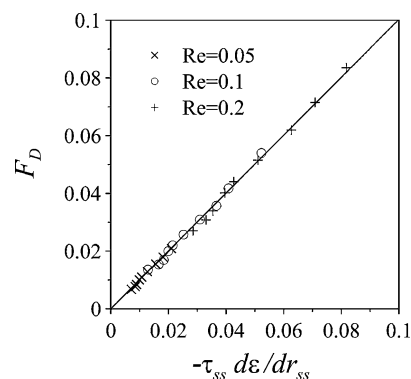


Fig. 5 Validation of the proposed relation between the hydrodynamic forces and the gradients of the dissipation rate: $F_D = -\tau_{ss} d\epsilon/dr_{ss}$. Here, the numerically calculated force, F_D , plotted as a function of $-\tau_{ss} d\epsilon/dr_{ss}$ for different Reynolds numbers, Re , falls nicely onto a straight line with slope of unity. The computational errors for the characteristic time are within the size of symbols representing their values on the plot.

particle speed (Fig. 4c) is the result of a transient, inertial lift force of the type described by Rubinow and Keller³⁶ for a rotating sphere translating relative to the fluid in a direction perpendicular to its axis of rotation (*cf.* Fig. 4b). Qualitatively, the origin of this force may be understood as a consequence of Bernoulli's principle, whereby the fluid flows more rapidly over one side of the rotating sphere than over the other; therefore, there is a pressure difference acting on the sphere in the direction, $F_L = \omega \times V$. Importantly, this force initially opposes the acceleration of the sphere towards its new steady-state velocity but eventually gives way to the expected increase in ΔV as the particles move closer together. From the time evolution of ΔV , we find that $\Delta V(t) - \Delta V_0 \approx \exp(-t/\tau_{ss})$, (Fig. 4d), where τ_{ss} is the characteristic time used to relate the force and the dissipation rate—even for different steady-states, r_{ss} , and Reynolds numbers, Re (Fig. 5).

Qualitatively, τ_{ss} is the time required for the particle to accelerate from its initial trajectory and begin its quasi-steady approach towards the new steady-state. This is best illustrated by examining the difference in the radial velocity components of the perturbed and unperturbed trajectories, $\Delta V_r = V_r' - V_r$ (Fig. 4e). Here, we see that the particle accelerates rapidly, with a characteristic time scale, τ_{ss} , before reaching a quasi-steady velocity with which it gradually approaches the new steady-state (note: the latter requires a long time and is not illustrated in the figure). Importantly, because this time is related to the inertial acceleration of the particle, it depends linearly on the Reynolds number, Re , (Fig. 4f)—indeed, as it should in order to relate the force (also linearly proportional to Re) and the dissipation rate (independent of Re). Furthermore, this acceleration time is a monotonically increasing function of the initial steady-state radial position, r_{ss} .

From a more general perspective, the characteristic time, τ_{ss} , provides a measure of the difference between the actual perturbed trajectory and a hypothetical quasi-static trajectory, in which the particles would evolve slowly enough as to maintain the steady-state flow field. For example, when the particles are close to one another, they interact more strongly, such that changes in the flow field relax to steady-state rapidly, and τ_{ss} is small. For particles far apart, however, they interact only weakly

and it requires more time for the system to relax to steady-state; consequently, τ_{ss} is large. This interpretation of τ_{ss} in terms of differences between “real” trajectories and quasi-static trajectories may potentially prove useful in the generalization of the proposed relation between forces and dissipation to systems with more assembling components and/or different types of dissipative interactions.

Conclusions

In summary, we investigated the relation between energy dissipation and the forces mediating self-assembly in the prototypical DySA system of magneto-hydrodynamic SA. Through numerical simulation of the system’s dynamics, we found that hydrodynamic forces between the rotating particles are directly proportional to the gradient of the energy dissipation with respect to a coordinate characterizing the steady-state assembly. The constant of proportionality linking these otherwise disparate quantities is a characteristic time describing the response of the steady-state particle velocities to small, externally applied perturbations. Importantly, this previously unreported connection between forces and energy dissipation enables a potentially useful method for the calculation of forces or dissipation rates in the context of DySA. For example, if the externally applied forces, F_C , are known, the characteristic times, τ_{ss} , may be estimated experimentally by perturbing the steady-state configuration and monitoring the trajectories of the components transitioning to a new steady-state (in direct analogy to the methodology presented here). The local gradients of the dissipation rates can then be found from $\nabla\epsilon = -F_D/\tau_{ss} = F_C/\tau_{ss}$, and when integrated over different steady-states, can be used to reconstruct the system’s dissipation “landscape”, ϵ . Conversely, if the dissipation rates are measurable experimentally (e.g., via calorimetric measurements on the steady dissipative assemblies), the proposed relation enables the calculation of the various dissipative forces guiding the organization of the system. Of course, further work is needed to investigate the validity of this relation for systems comprising more components (initial results indicate that it holds for three-component systems) and for different types of dissipative interactions.

Acknowledgements

We are grateful to Professor M. R. Maxey and Professor E. Climent for the code of the FCM method used in the simulations. Parts of the calculations were performed at the Poznań Supercomputing and Networking Center (PCSS).

References

- 1 G. M. Whitesides and B. Grzybowski, *Science*, 2002, **295**, 2418–2421.
- 2 M. Fialkowski, K. J. M. Bishop, R. Klajn, S. K. Smoukov, C. J. Campbell and B. A. Grzybowski, *J. Phys. Chem. B*, 2006, **110**, 2482–2496.
- 3 B. Alberts, A. Johnson, J. Lewis, M. Raff, K. Roberts and P. Walter, *Molecular Biology of the Cell*, Garland, New York, 2002.
- 4 E. O. Budrene and H. C. Berg, *Nature*, 1991, **349**, 630–633.
- 5 E. O. Budrene and H. C. Berg, *Nature*, 1995, **376**, 49–53.
- 6 E. Bonabeau, M. Dorigo and G. Theraulaz, *Nature*, 2000, **406**, 39–42.
- 7 D. H. Cushing and F. R. H. Jones, *Nature*, 1968, **218**, 918–920.
- 8 J. K. Parrish and L. Edelstein-Keshet, *Science*, 1999, **284**, 99–101.

- 9 J. C. Love, L. A. Estroff, J. K. Kriebel, R. G. Nuzzo and G. M. Whitesides, *Chem. Rev.*, 2005, **105**, 1103–1169.
- 10 D. Witt, R. Klajn, P. Barski and B. A. Grzybowski, *Curr. Org. Chem.*, 2004, **8**, 1763–1797.
- 11 M. Eddaoudi, D. B. Moler, H. L. Li, B. L. Chen, T. M. Reineke, M. O’Keeffe and O. M. Yaghi, *Acc. Chem. Res.*, 2001, **34**, 319–330.
- 12 A. M. Kalsin, M. Fialkowski, M. Paszewski, S. K. Smoukov, K. J. M. Bishop and B. A. Grzybowski, *Science*, 2006, **312**, 420–424.
- 13 Y. N. Xia, B. Gates, Y. D. Yin and Y. Lu, *Adv. Mater.*, 2000, **12**, 693–713.
- 14 M. Boncheva, R. Ferrigno, D. A. Bruzewicz and G. M. Whitesides, *Angew. Chem., Int. Ed.*, 2003, **42**, 3368–3371.
- 15 G. Helgessen, E. Svasand and A. T. Skjeltorp, *J. Phys.: Condens. Matter*, 2008, **20**.
- 16 R. M. Capito, H. S. Azevedo, Y. S. Velichko, A. Mata and S. I. Stupp, *Science*, 2008, **319**, 1812–1816.
- 17 G. Nicolis and I. Prigogine, *Self-Organization in Nonequilibrium Systems: From Dissipative Structures to Order Through Fluctuations*, Wiley, New York, 1977.
- 18 This refers to the so-called linear regime of nonequilibrium thermodynamics, in which the fluxes are linear functions of the various thermodynamic forces, and the assumption of local thermodynamic equilibrium remains valid.
- 19 S. R. d Groot and P. Mazur, *Nonequilibrium thermodynamics*, Dover, New York, 1984.
- 20 S. Kin and S. J. Karrila, *Microhydrodynamics: Principles and Selected Applications*, Dover, New York, 2005.
- 21 D. G. Christopherson and D. Dowson, *Proc. R. Soc. London, Ser. A*, 1959, **251**, 550–564.
- 22 B. Y. Ballal and R. S. Rivlin, *Arch. Ration. Mech. Anal.*, 1976, **62**, 237–294.
- 23 B. A. Grzybowski, X. Y. Jiang, H. A. Stone and G. M. Whitesides, *Phys. Rev. E*, 2001, **64**, 011603.
- 24 B. A. Grzybowski, H. A. Stone and G. M. Whitesides, *Nature*, 2000, **405**, 1033–1036.
- 25 B. A. Grzybowski, H. A. Stone and G. M. Whitesides, *Proc. Natl. Acad. Sci. U. S. A.*, 2002, **99**, 4147–4151.
- 26 B. A. Grzybowski and G. M. Whitesides, *J. Phys. Chem. B*, 2001, **105**, 8770–8775.
- 27 B. A. Grzybowski and G. M. Whitesides, *J. Phys. Chem. B*, 2002, **106**, 1188–1194.
- 28 B. A. Grzybowski and G. M. Whitesides, *J. Chem. Phys.*, 2002, **115**, 8571–8577.
- 29 B. A. Grzybowski and G. M. Whitesides, *Science*, 2002, **296**, 718–721.
- 30 E. Climent, K. Yeo, M. R. Maxey and G. E. Karniadakis, *J. Fluids Eng.-Trans. ASME*, 2007, **129**, 379–387.
- 31 D. Liu, M. Maxey and G. E. Karniadakis, *J. Microelectromech. Syst.*, 2002, **11**, 691–702.
- 32 S. Lomholt and M. R. Maxey, *J. Comput. Phys.*, 2003, **184**, 381–405.
- 33 Interestingly, the dissipation rate is well approximated by the Stokes solution ($Re = 0$),³⁴ and the inclusion of finite fluid inertia introduces only small corrections (Fig. 3b). Thus, in the Stokes limit, F_D is identically zero, and the particles are free to orbit each other for any separation, r_{ss} , regardless of the magnitude of the dissipation rate, ϵ . It is only through the inclusion of finite fluid inertia that the system “chooses” from the infinite possibilities and evolves towards the state of minimum dissipation. This characteristic is also shared by the hydrodynamic problems described in the Introduction: sphere falling through a cylinder, (ii) flow between two rotating cylinders.
- 34 M. E. O’neill, *Appl. Sci. Res.*, 1970, **21**, 452–466.
- 35 This value was chosen to be large enough such that τ_{ss} could be measured over the “noise” of the simulation but otherwise as small as possible. Specifically, we found that the perturbing force $\Delta F = 0.01 F_D$ gave the most reliable results.
- 36 S. I. Rubinow and J. B. Keller, *J. Fluid Mech.*, 1961, **11**, 447–459.
- 37 S. Soh, K. J. M. Bishop and B. A. Grzybowski, *J. Phys. Chem. C.*, 2008, in press.
- 38 R. Klajn, K. J. M. Bishop and B. A. Grzybowski, *Proc. Natl. Acad. Sci. U. S. A.*, 2007, **104**, 10305–10309.
- 39 R. Klajn, K. J. M. Bishop, M. Fialkowski, M. Paszewski, C. J. Campbell, T. P. Gray and B. A. Grzybowski, *Science*, 2007, **316**, 261–264.